

PHYSICS

Exploring complex graphs using three-dimensional quantum walks of correlated photons

Max Ehrhardt¹, Robert Keil², Lukas J. Maczewsky¹, Christoph Dittel^{3,4}, Matthias Heinrich¹, Alexander Szameit^{1*}

Graph representations are a powerful concept for solving complex problems across natural science, as patterns of connectivity can give rise to a multitude of emergent phenomena. Graph-based approaches have proven particularly fruitful in quantum communication and quantum search algorithms in highly branched quantum networks. Here, we introduce a previously unidentified paradigm for the direct experimental realization of excitation dynamics associated with three-dimensional networks by exploiting the hybrid action of spatial and polarization degrees of freedom of photon pairs in complex waveguide circuits with tailored birefringence. This testbed for the experimental exploration of multiparticle quantum walks on complex, highly connected graphs paves the way toward exploiting the applicative potential of fermionic dynamics in integrated quantum photonics.

INTRODUCTION

Complex networks occur across many different fields of science, ranging from biological signaling pathways and biochemical molecules exhibiting efficient energy transport (1) to neuromorphic circuits and social interactions in the ever-expanding World Wide Web (2). In general, such structures are modeled by graphs, whose complexity is dictated by the number of nodes and linkage patterns between them. Crucially, any physical representation of a graph is constrained by the fact that both of these need to be arranged in three-dimensional (3D) space. A marked example of the resulting scaling behavior, which is highly unfavorable for physical simulation, is the human brain, in which the already staggering number of 80 billion neurons is dwarfed by the 100 trillion synapses enabling the flow of signals between them (3). Despite the comparably minuscule number of nodes, discrete quantum systems face a similar challenge: Complex network topologies with a high degree of connectivity allow for potent applications (4) such as efficient multipartite quantum communication (5) or search algorithms (6, 7), but the physical implementation of such networks has—so far—been constrained to two dimensions.

The transport properties of connected graphs are usually studied in the framework of quantum walks (QWs). The paradigmatic case of a linear 1D chain has been implemented on a wide range of different technological platforms (8–14). Whereas the dynamics of single-particle QWs can be understood through classical interference phenomena (15), QWs of multiple indistinguishable particles (16) fundamentally exceed this framework: Their nonclassical correlations arising from multiparticle quantum interference (17) enable novel applications in quantum computation (18), e.g., a solver for the graph isomorphism problem (19). Moreover, virtual multidimensional graphs can be obtained by interpreting multiparticle systems as single walkers (20, 21). Using the dimensionality of experimental platforms—supporting the implementation of graphs—as a resource for increasing

the vertices' connectivity sheds light onto coherence phenomena ranging from biological systems (22–24) to graph theory problems (21, 25) and enables quantum search algorithms (26). Simultaneously leveraging both methods—multiple walkers and 2D single-particle graphs—brings the experimental realization of graphs with even higher complexity into reach (27). Unfortunately, spatial dimensions are a rather sparse commodity, a fact that is often exacerbated by practical limitations of technological platforms. Internal degrees of freedom of the walkers can mitigate these constraints by providing artificial dimensions (28). In the context of (classical wave) photonics, this strategy has enabled the implementation of specific scenarios via coupled sets of physical states (29, 30) or additional parameter dependencies in the system dynamics (31). The development of methods that are applicable to multiple walkers and genuinely increase the dimensionality of any physically implemented underlying graph remains an open challenge of crucial importance.

In this work, we demonstrate controlled QWs of correlated photons on 3D graphs. We realize the graph structure by means of a novel hybrid approach: 2D photonic lattices of spatially coupled waveguides are inscribed into fused silica by femtosecond laser writing (32), while one synthetic dimension is encoded in the photons' polarization. The dynamics within the synthetic dimension are established by harnessing the intrinsic birefringent properties of the elliptical waveguides that historically have been used as polarization active cores of individual single-mode optical fibers (33). By appropriately rotating the waveguides' respective fast principal axes with respect to an external reference frame, continuous coupling between the two orthogonal polarization states takes place. In this vein, a single waveguide yields coherent population oscillations between the polarization modes (Fig. 1A). Whereas the external reference frame is arbitrary for an isolated core, the spatial arrangement of coupled waveguide removes this ambiguity. As such, lattices can be transformed into bilayer versions of themselves by an appropriate orientation of their elliptical cores (Fig. 1B). Notably, following this strategy to implement higher-dimensional graphs naturally gives rise to hypercube (HC) symmetries that have recently been predicted to leave their distinct signature on the evolution of correlated photon pairs (34). To discern the fingerprints of quantum interference, we use the nonclassicality $\nu = C_{\text{ind}}/C_{\text{dis}} - 1$, contrasting the measured coincidence count rates between indistinguishable (C_{ind}) and distinguishable

Copyright © 2021
The Authors, some
rights reserved;
exclusive licensee
American Association
for the Advancement
of Science. No claim to
original U.S. Government
Works. Distributed
under a Creative
Commons Attribution
NonCommercial
License 4.0 (CC BY-NC).

¹Institut für Physik, Universität Rostock, Albert-Einstein-Straße 23 18059 Rostock, Germany. ²Institut für Experimentalphysik, Universität Innsbruck, Technikerstr. 25, 6020 Innsbruck, Austria. ³Physikalisches Institut, Albert-Ludwigs-Universität Freiburg, Hermann-Herder-Str. 3, 79104 Freiburg, Germany. ⁴EUCOR Centre for Quantum Science and Quantum Computing, Albert-Ludwigs-Universität Freiburg, Hermann-Herder-Str. 3, 79104 Freiburg, Germany.

*Corresponding author. Email: alexander.szameit@uni-rostock.de

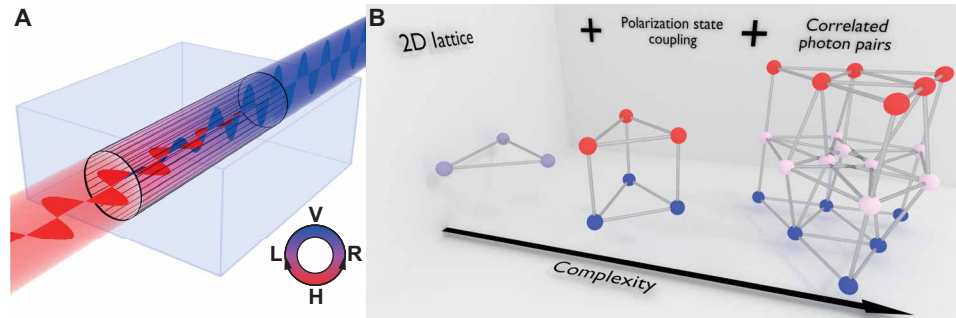


Fig. 1. Using polarization as an additional synthetic dimension. (A) A single waveguide with tailored birefringence coherently couples its horizontally (red) and vertically (blue) polarized modes of the electromagnetic field. (B) Planar graphs (left) acquire an additional dimension due to the coupling of two polarization states (middle). The Hilbert space of photon pairs on 3D graphs takes the form of a yet more complex graph (right).

photons (C_{dis}), respectively. We further examine conditions for the selective suppression ($\nu < 0$) or enhancement ($\nu > 0$) of output states, revealing bosonic and fermionic behavior on certain subgraphs, respectively. Last, we show that our technique allows for the control of both strength and sign of the coupling along the synthetic dimension and use negative couplings to selectively induce partial breaking of the graph's HC symmetry. Our approach opens new avenues for the experimental exploration of quantum dynamics on highly complex graphs that play an essential role in numerous disciplines of science.

RESULTS AND DISCUSSION

To illustrate the working principle, we first show that the hallmark of two-particle interference, the Hong-Ou-Mandel (HOM) effect (35), arises in the polarization degree of freedom of a single waveguide. Direct laser-written waveguides in fused silica are intrinsically birefringent (36) and therefore can be individually described by the Hamiltonian

$$\hat{H} = \beta_s \hat{a}_s^\dagger \hat{a}_s + \beta_f \hat{a}_f^\dagger \hat{a}_f \quad (1)$$

with the bosonic annihilation (creation) operators $\hat{a}_{s/f}^{(\dagger)}$ for photons on the slow/fast principal axis with propagation constant $\beta_{s/f}$, respectively. As schematically shown in Fig. 2A, these axes may be oriented at an angle α toward the horizontal/vertical (H/V) frame of reference (37). Any value of α that deviates from integer multiples of $\pi/2$ then entails dynamics in the polarization states of photons propagating along the z direction according to the Heisenberg equation of motion (see section S1 for details)

$$i \frac{d}{dz} \begin{pmatrix} \hat{a}_H^\dagger \\ \hat{a}_V^\dagger \end{pmatrix} = \begin{pmatrix} \bar{\beta} + \Delta \cdot \cos 2\alpha & \Delta \cdot \sin 2\alpha \\ \Delta \cdot \sin 2\alpha & \bar{\beta} - \Delta \cdot \cos 2\alpha \end{pmatrix} \begin{pmatrix} \hat{a}_H^\dagger \\ \hat{a}_V^\dagger \end{pmatrix} \quad (2)$$

where $\bar{\beta} = (\beta_f + \beta_s)/2$ describes the mean propagation constant and $\Delta = (\beta_s - \beta_f)/2$ represents the strength of birefringence. Notably, this mathematical structure is fully equivalent to the description of the dynamics in a coupled and detuned two-waveguide system. In our polarization-coupling regime, the counterpart of the propagation constants' mismatch, $\Delta \cdot \cos 2\alpha$, and coupling strength, $\Delta \cdot \sin 2\alpha$, can both be adjusted via the birefringence Δ (36) and the rotation angle α (37). Here, the case of $\alpha = 45^\circ$ —entailing equally large propagation constants for the H/V modes—appears particularly interesting because the system behaves analogously to a phase-matched

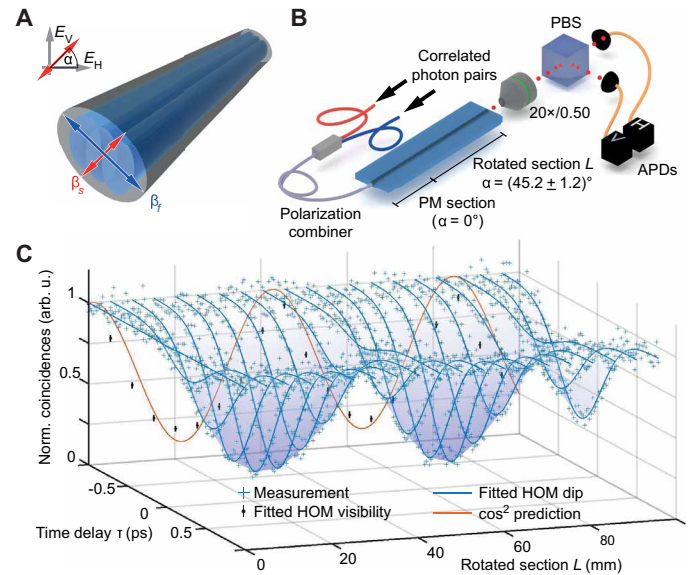


Fig. 2. Quantum interference in a polarization coupler. (A) Triple-pass femto-second laser-written waveguides enable control over both magnitude and orientation of the birefringence. Changes to the angle α of the slow axis allow for polarization-maintaining (PM) sections to be included at will. (B) Correlated photon pairs combined in a single waveguide exhibit HOM interference due to a coupling of the horizontal and vertical polarization modes in a section with rotated fast and slow axes of length L . (C) Coincidence rate measured as a function of the time delay τ between the photons' arrival time and length L of the rotated section. The displayed \cos^2 prediction fits the data for $\tau = 0$ and a visibility limited only by the photon source to $(92.3 \pm 1.1)\%$ (see Materials and Methods for details). The largest observed visibility was $(84.2 \pm 2.1)\%$. arb. u., arbitrary units.

directional coupler, or beam splitter, with a tunneling amplitude $t = \sin(z \cdot \Delta)$, depending on the propagation length z . Similar to conventional couplers (38), the performance of this component can be evaluated by measuring the quantum interference (35) between the polarization states. To this end, a polarization-duplexed input state $|H, V\rangle \equiv \hat{a}_H^\dagger \hat{a}_V^\dagger |0\rangle$ is synthesized from photon pairs generated by spontaneous parametric down-conversion (SPDC) and injected into a polarization-maintaining (PM) waveguide ($\alpha = 0$), in which a rotated section with angle $\alpha = (45.2 \pm 1.2)^\circ$ and length L is embedded (see Fig. 2B). As the time delay τ between the photons at the injection facet is varied, the coincidence counts of two avalanche

photodiodes (APDs; registering output photons in H and V polarization, respectively) are recorded. The resulting 2D “HOM landscape,” obtained for 20 different lengths L , is shown in Fig. 2C. Along the cross section $\tau = 0$, the characteristic $\cos^2(2L \cdot \Delta)$ oscillation of the conventional two-mode coupler is reproduced with HOM interference visibilities (for fixed L) of up to 0.842 ± 0.021 .

With the necessary tools at hand, we proceed to extend a system of two spatially coupled waveguides (evanescent coupling rate κ) to a square lattice encoded in space and polarization (Fig. 3A): Note that conventional waveguide couplers are typically designed for one specific input polarization, and the photon dynamics for the other principal axis tend to yield a different splitting ratio as dictated by the difference in the polarization-dependent coupling strength between the two channels. Nevertheless, the orientation of their respective fast or slow axes tends to align with the plane defined by the position of the two cores. In contrast, here, we use a 45° rotation of the principal axes with respect to this plane to enable simultaneously spatial coupling and a well-defined cross-talk between the polarization states within a given waveguide. Moreover, this configuration also serves to mitigate the polarization-dependent mismatch of the

coupling strengths between the waveguides. Details on how birefringence establishes the additional dimension of the graph structure are provided in section S2. By choosing the waveguide spacing such that $\kappa = \Delta$, the resulting square lattice constitutes a 2D HC (34) for which the unitary transfer matrix after a coupling length $L = \pi/(4\Delta)$ reads

$$U = \left(\frac{1}{\sqrt{2}} \begin{pmatrix} 1 & i \\ i & 1 \end{pmatrix} \right)^{\otimes 2} \quad (3)$$

where $(\dots)^{\otimes 2}$ denotes the tensor square applied to the transfer matrix of a two-site coupler with equal output amplitudes for a single-site excitation, also designated as HC symmetry factor. In our experiment, this is accomplished for a propagation length $L = 6.92$ cm. We investigate the collective dynamics of two-photon input states for all possible arrangements with, at most, one photon per site. After the transformation governed by the square lattice, the polarization components are separated by two on-chip polarization beam splitters (PBSs), with the photons subsequently detected by APDs. For distinguishable photons, the equally strong couplings between the

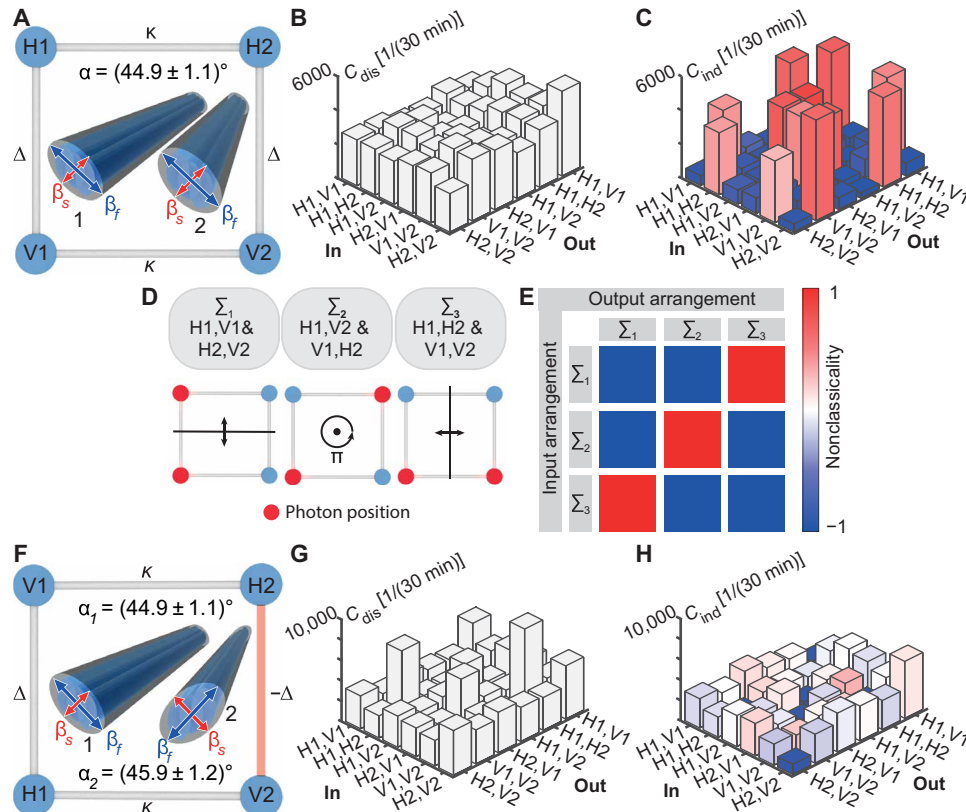


Fig. 3. Square lattices in a single spatial dimension. (A) A pair of birefringent waveguides with slow axes at $\alpha = 45^\circ$ implements a square graph structure with coupling strengths $\kappa = (\kappa_f + \kappa_s)/2$ (averaged coupling strength between slow/fast axes) between waveguides 1 and 2, and $\Delta = (\beta_s - \beta_f)/2$ between polarizations H and V. (B) Measured coincidence matrix of two distinguishable photons. For coupling parameters $\kappa = \Delta$, classical (single-particle) dynamics yields a nearly uniform distribution after a propagation length of $L = \pi/(4\Delta)$. (C) Coincidence rates for indistinguishable photons. In addition to the count rates (height), the nonclassicality ν is color-coded to indicate enhancement (red) and suppression (blue) by quantum (two-particle) interference. (D) Illustration of the self-inverse symmetry operations Σ_1 , Σ_2 , and Σ_3 on the 2D HC graph, leaving the two-photon arrangements (indicated by red spheres) invariant. (E) Nonclassicality for combinations of initial-final photon arrangements captured by the suppression laws associated with Σ_1 , Σ_2 , and Σ_3 . The red (blue) squares indicate enhanced (reduced) probabilities of the corresponding input-output transition. (F) Clockwise ($\alpha = +45^\circ$) and counterclockwise ($\alpha = -45^\circ$) rotated principal axes implement a square lattice with negative coupling strength between two sites. For equal coupling strengths $\kappa = \Delta$ (κ : coupling strength between fast and slow axes of different waveguides) and propagation length $L = \pi/(4\Delta)$, we measure the coincidence rates for (G) distinguishable and (H) indistinguishable photon pairs.

lattice sites result in a uniform output probability distribution across the entire lattice (Fig. 3B). In contrast, as illustrated by the color-coded nonclassicality in Fig. 3C, for indistinguishable photons, destructive and constructive quantum interference causes full suppression ($\nu \approx -1$) and pronounced enhancement ($\nu > 0$), respectively. Upon closer examination, ν appears closely related to the three self-inverse symmetries Σ_1 (mirror symmetry of the polarization coupler), Σ_2 (π -rotation of the square lattice), and Σ_3 (mirror symmetry of the waveguide coupler) of the HC graph illustrated in Fig. 3D: In accordance with the HC suppression law (39–41), the symmetry operation that leaves the input state invariant determines the suppression of four output states (different ones for each symmetry), while the detection probability of all other output states appears enhanced compared to distinguishable particles (cf. Fig. 3E). The suppression of the Σ_1 - Σ_1 and Σ_3 - Σ_3 input-output combinations is closely related to HOM interference in the polarization or waveguide coupler, respectively. In this vein, photons are launched and observed in coupled sites and tend to bunch in one of the two sites irrespective of joint changes to the waveguide and polarization. The other cases arise from the interference of all photon-pair amplitudes traversing both lattice dimensions. As predicted by the HC suppression laws (see section S3), phase bookkeeping of all two-photon trajectories for the Σ_1 - Σ_2 , Σ_2 - Σ_1 , Σ_2 - Σ_3 , and Σ_3 - Σ_2 input-output combinations reveals pairwise occurring paths with a phase difference of π , and therefore, fully destructive quantum interference emerges (34).

In addition to increasing the dimensionality of lattices, Eq. 2 allows for even more general coupling scenarios: Combining waveguides with clockwise and counterclockwise rotated fast axes (see Fig. 3F), the polarization coupling terms acquire opposite signs, thereby providing a direct route to implement negative coupling strengths without the need for complex background lattice engineering or ancillary waveguides (42, 43). Notably, an $\alpha = \pm 45^\circ$ arrangement also enables coupling between the V-polarized mode of one waveguide to the H-polarized mode of the other, and vice versa (see section S4 for details). Following this approach, we implement a polarization-encoded square lattice in which one of the polarization couplings has a negative sign, thereby breaking the underlying symmetry of the graph with special implications: Individual photons cannot be found on the diagonally opposite site of their starting position as a consequence of destructive interference caused by the different signs of coupling strengths. The resulting output statistics for distinguishable and indistinguishable photons are shown in Fig. 3 (G and H, respectively) and clearly differ from those obtained with positive couplings only. Because of the absence of photons on specific sites, for each input arrangement, the nonclassicality in Fig. 3H indicates suppression only for a single output state, whereas all other output states show no substantial fingerprints of quantum interference ($\nu \approx 0$).

In a final set of experiments, we implement a 3D QW. An equilaterally coupled triangle of identical, birefringent waveguides (Fig. 4A) is transformed into a triangular prism whose unitary transfer matrix reads

$$U = \frac{1}{\sqrt{2}} \begin{pmatrix} 1 & i \\ i & 1 \end{pmatrix} \otimes A \quad (4)$$

where A is the transfer matrix of the triangular subgraph (see section S2 for details). Compared to Eq. 3, the tensor power of the HC symmetry factor is reduced by 1, and in general, only a single HC dimension is established in the polarization degree of freedom.

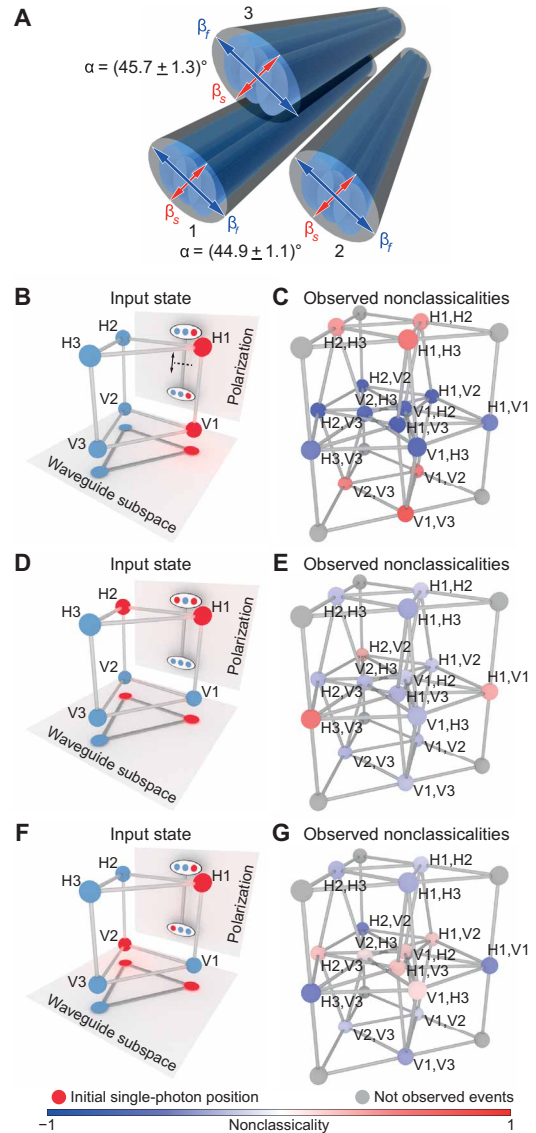


Fig. 4. 3D graph in two spatial dimensions. (A) The graph structure of a triangular prism is realized with three coupled birefringent waveguides arranged in the shape of an equilateral triangle. (B, D, and F) Two-photon input states are illustrated by red nodes on the single-photon graphs and the respective projections on the polarization and waveguide subspaces. (C, E, and G) The corresponding experimentally observed nonclassicalities (coincidence rates are available in fig. S4) are color-coded on a two-photon graph representation for the input states shown on the left-hand side. Gray nodes indicate output states with both photons in the same waveguide and polarization, which are inaccessible in the present experimental setting without photon number-resolving detection.

The input state $|H1, V1\rangle$ (one H- and one V-polarized photon injected into waveguide 1) is invariant under the HC symmetry, as indicated by the mirror-symmetric projection into the polarization subspace in Fig. 4B. The polarization subspace contains a two-site coupler that plays the dominant part for the observed quantum interference (Fig. 4C): Output states with one photon in each H and V polarization (shown in the central layer of the 3D two-photon graph in Fig. 4C) appear suppressed, such that both photons must exit the structure in the same polarization state (top and bottom

layers in Fig. 4C). In contrast, the input states $|H1, H2\rangle$ (see Fig. 4D) and $|H1, V2\rangle$ (see Fig. 4F) break the mirror symmetry in the polarization subspace and the HC symmetry-induced suppression of quantum states vanishes. For instance, $|H1, H2\rangle$ partially suppresses the probability of finding both photons in different waveguides and, at the same time, enhances bunching behavior of orthogonally polarized photons in the same waveguide (Fig. 4E). This property is inextricably linked to the bosonic QW on the triangular graph in the waveguide subspace in Fig. 4D. These observations are independent of the polarization, because single-photon hopping in the polarization subspace in this case only accumulates irrelevant phases for the two-photon interference and the influence of the HC structure vanishes (see section S3 for details). The same applies if the photons are launched in the input state $|H1, V2\rangle$ and subsequently observed both in the same polarization (H or V). In this case, only one photon changes the site in the polarization subspace and accumulates an irrelevant phase for quantum interference. Consequently, the top and bottom layers of the two-photon graph in Fig. 4G exhibit the same signatures of quantum interference as for the input state $|H1, H2\rangle$, which are only affected by the spatial two-photon dynamics. The input state $|H1, V2\rangle$ leads to a purely fermionic anti-bunching behavior for output photons with different polarizations (details are provided in section S3): Both photons, despite being bosons, inevitably end up in different waveguides, as evidenced by the full suppression and enhancement of the corner and remaining nodes in the central layer of the two-photon graph in Fig. 4F, respectively. For different output polarization, both photons either maintain or change their respective polarizations. Whereas maintaining the polarization does not introduce additional phases to the two-photon wave function, the joint polarization change can be interpreted as a permutation operation in the two-photon state in the waveguide subspace. The associated phase shift of π gives rise to antisymmetric features of the two-particle wave function (44). In other words, the two bosonic walkers behave as fermionic walkers on the equilateral triangular waveguide lattice and adhere to the degeneracy prohibition expressed by the Pauli principle.

Notably, this division into bosonic and fermionic behavior is a direct consequence of the underlying HC structure and, as such, is not restricted to the triangular subgraph geometry investigated here: The same characteristics would hold for any other subgraph structure. Thus, the HC suppression law and the Pauli principle are the

general mechanisms leading to the suppression of output states on the bilayer lattice (Fig. 5). In turn, specifically designed waveguide lattices (e.g., Fig. 3A) can selectively instantiate suppression mechanisms on the basis of bosonic or fermionic two-particle interference on the waveguide subspace.

The exploration of quantum dynamics on complex graphs plays an essential role in numerous disciplines of science. However, as the dimensionality increases, their experimental implementation becomes an ever more challenging task. We introduced a novel approach to expand the dimensionality of photonic lattices by using the polarization degree of freedom as an additional synthetic dimension that is applicable to current approaches for increasing the vertices' connectivity in a spatial configuration (45, 46). As demonstrated by the observation of HOM interference in a single waveguide with appropriately tailored birefringence, the dynamical features introduced by the additional dimension are in perfect agreement with the characteristic

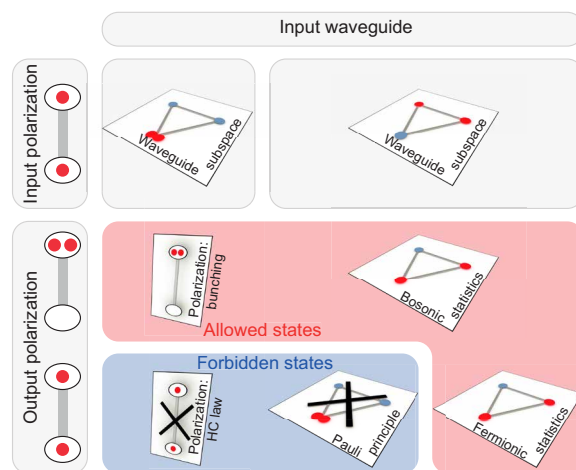


Fig. 5. Summary of forbidden and allowed output states. Two photons are launched in different polarization sites (each photon position is indicated by a red node) and in different waveguides (right column) or in the same waveguide (middle column). We classify the possible final two-photon arrangements associated with their input state and their observed hallmarks of quantum interference in allowed (red frame) and forbidden states (blue frame) and same (middle row) and different (bottom row) output polarization states.

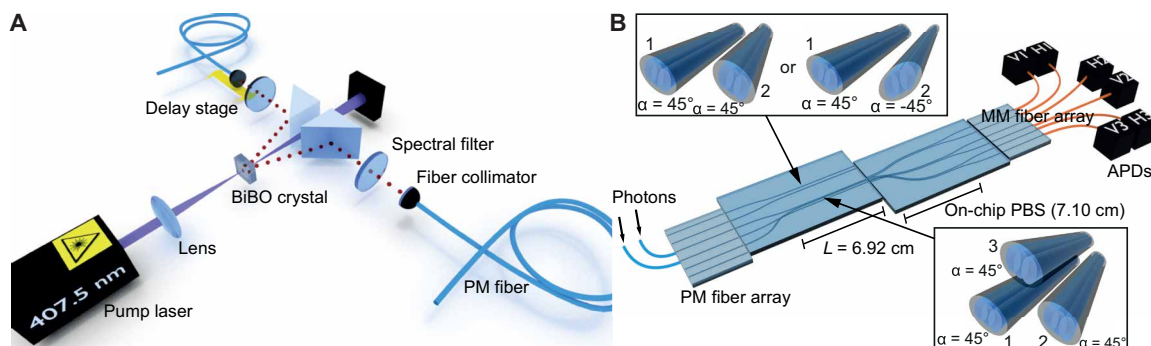


Fig. 6. Experimental setup. (A) Correlated photon pairs are generated by type I SPDC. A BiBO crystal is pumped with a focused laser beam. The two horizontally polarized photons and the pump beam are separated with two prisms. After passing spectral filters, the photons are collected by PM fibers. The time delay τ between the photons is set by a delay stage. (B) The generated photon pairs are launched either on the fast or on the slow axes of the fibers in the PM fiber array. After the photons evolve in waveguide arrangements of two or three waveguides with rotated principal axes, they pass an integrated PBS on a second sample. In the end, the photons are collected with multimode (MM) fibers and detected with APDs.

quantum dynamics expected from spatial dimensions. In further proof-of-principle experiments, we observed quantum interference in fully controlled QWs of correlated photons on 3D graphs, a long-standing goal in quantum photonics. Beyond increasing the dimensionality of a given graph configuration, our technique naturally allows for the implementation of negative couplings without the need for any ancillary structures (42, 43). Along similar lines, polarization-coupled lattices can readily establish anti-bunching of photons—a key ingredient for probing complex fermionic QWs and harnessing their unique suppression behavior beyond conventional methods based on polarization-entangled two-photon sources that explicitly allocate fermionic or bosonic statistics according to an input state's chosen exchange symmetry (47, 48). As a direct result from the here established framework, a number of fascinating opportunities arise beyond the context of correlated QWs: The quantum dynamics (both single-particle and multiparticle) of bilayer 2D materials can be emulated in photonic model systems, and the impact of nonlinearities on wave packets evolving on complex graphs becomes experimentally accessible by using bright light pulses and the Kerr nonlinearity. Last, graphs with periodic boundaries or nontrivial topologies (49) as well as further topological questions such as the graph isomorphism problem can now be addressed more efficiently on optical platforms.

MATERIALS AND METHODS

Waveguide fabrication and classical characterization

We fabricate nearest-neighbor coupled waveguide circuits using the direct laser writing technique (32). Femtosecond pulses at $\lambda = 800$ nm with a 200 – kHz repetition rate were focused in fused silica with a 40 \times (NA = 0.65) or 20 \times (NA = 0.35) objective to fabricate the lattices for the HOM experiment (see Fig. 2) or the 2D and 3D QWs (see Figs. 3 and 4, respectively).

The rotation of the principal axis of a waveguide is realized by triplicated waveguides with a transverse offset of 3 and 5 μm oriented at an angle of 31 $^\circ$ and 10 $^\circ$ with respect to the horizontal plane for the 40 \times and 20 \times objective, respectively. We determine the orientation of the principal axis α as well as the strength of birefringence Δ with the method of two crossed polarizers (50). Simultaneously rotating the orientation of the first and second PBS by θ (this maintains the crossed orientation of the polarizers), the intensity ratio of the transmitted light I_T and total intensity I_{total} , measured with two photo diodes, reads

$$\frac{I_T}{I_{\text{total}}} = \sin^2(2(\theta - \alpha)) \sin^2(L \cdot \Delta) \quad (5)$$

with the length L of the waveguide. The angle α can now be determined by the minimum in the recorded data. Using different lengths L of the 45 $^\circ$ rotated part (e.g., realized to record the data in Fig. 2C) and fixed positions $\theta = 0^\circ$, the relatively transmitted intensity follows

$$\frac{I_T}{I_{\text{total}}} = \sin^2(L \cdot \Delta) \quad (6)$$

so that Δ can be reconstructed from the measurement.

Bi-photon creation and experiment

For the generation of photon pairs, we used a type I SPDC source (see Fig. 6A). A BiBO crystal is pumped by a 100 – mW laser diode

(Coherent OBIS, continuous wave) at $\lambda_p = 407.5$ nm. This produces wavelength-degenerate horizontally polarized photon pairs at $\lambda_s = 815$ nm, which are collected by PM fibers and subsequently routed to the sample. We adjust the delay τ in between the arrival times of the two photons at the sample with a delay stage. Indistinguishable photons are obtained by setting $\tau = 0$, whereas delays $|\tau| > 1$ ps yield distinguishable photons: According to the Gaussian fit of the HOM dips in Fig. 2C, a 1 – ps delay results in bunching of less than 0.7% photon pairs, which is negligible compared to the counting error in the case of less than 10,000 counts. For the characterization of the photons' indistinguishability, we record the HOM dip that reaches a visibility of up to $(92.3 \pm 1.1)\%$ as measured with a fiber-based beam splitter.

Our experimental setup (see Fig. 6B) allows us to launch photons from an SPDC source with either horizontal (H) or vertical (V) polarization. This feature is enabled by fiber mating sleeves that align the fast axis of the PM fiber from the SPDC source to either the fast or the slow axis of the PM fiber array with a pitch of 127 μm leading to the waveguide chip. Inside the sample, the laser-written waveguides start with a curved interface section to adiabatically reduce their transverse distance to the value associated with the desired spatial coupling. In this fan-in section, the principal axes are aligned to the PM fibers, such that they maintain H and V polarization. In contrast, the main section of the chip contains spatially coupled waveguides with rotated principal axes, which induce specific polarization coupling behavior and the desired lattice dynamics. Last, we implement one on-chip PBS (51) for each waveguide of our lattice. The functionality of this section is implemented by coupled pairs of waveguides with a precise mismatch of coupling strengths for H- and V-polarized light, respectively. In addition to the separation of polarizations, the individual PBSs are also gradually separated from each other. To avoid bending losses that might systematically skew the results of the photon counts, we choose a length of 7.10 cm for this fan-out. Each PBS was implemented to exceed a polarization contrast of 98% (classical characterization) in the respective output waveguides. The same PBS structure was designed to be used for all lattices investigated in this work.

SUPPLEMENTARY MATERIALS

Supplementary material for this article is available at <http://advances.sciencemag.org/cgi/content/full/7/9/eabc5266/DC1>

REFERENCES AND NOTES

1. M. Walschaers, J. Fernandez-de-Cossio Diaz, R. Mulet, A. Buchleitner, Optimally designed quantum transport across disordered networks. *Phys. Rev. Lett.* **111**, 180601 (2013).
2. S. N. Dorogovtsev, J. F. F. Mendes, Evolution of networks. *Adv. Phys.* **51**, 1079–1187 (2002).
3. R. W. Williams, K. Herrup, The control of neuron number. *Annu. Rev. Neurosci.* **11**, 423–453 (1988).
4. J. Biamonte, M. Faccin, M. De Domenico, Complex networks from classical to quantum. *Commun. Phys.* **2**, 53 (2019).
5. A. Acin, J. I. Cirac, M. Lewenstein, Entanglement percolation in quantum networks. *Nat. Phys.* **3**, 256–259 (2007).
6. G. D. Paparo, M. Müller, F. Comellas, M. A. Martin-Delgado, Quantum google in a complex network. *Sci. Rep.* **3**, 2773 (2013).
7. B. Hein, G. Tanner, Quantum search algorithms on a regular lattice. *Phys. Rev. A* **82**, 012326 (2010).
8. C. A. Ryan, M. Laforest, J. C. Boileau, R. Laflamme, Experimental implementation of a discrete-time quantum random walk on an NMR quantum information processor. *Phys. Rev. A* **72**, 062317 (2005).
9. H. Schmitz, R. Matjeschek, C. Schneider, J. Glueckert, M. Enderlein, T. Huber, T. Schaetz, Quantum walk of a trapped ion in phase space. *Phys. Rev. Lett.* **103**, 090504 (2009).

10. M. Karski, L. Förster, J.-M. Choi, A. Steffen, W. Alt, D. Meschede, A. Widera, Quantum walk in position space with single optically trapped atoms. *Science* **325**, 174–177 (2009).
11. D. Bouwmeester, I. Marzoli, G. P. Karman, W. Schleich, J. P. Woerdman, Optical Galton board. *Phys. Rev. A* **61**, 013410 (1999).
12. F. Zähringer, G. Kirchmair, R. Gerritsma, E. Solano, R. Blatt, C. F. Roos, Realization of a quantum walk with one and two trapped ions. *Phys. Rev. Lett.* **104**, 100503 (2010).
13. B. Do, M. L. Stohler, S. Balasubramanian, D. S. Elliott, C. Eash, E. Fischbach, M. A. Fischbach, A. Mills, B. Zwickl, Experimental realization of a quantum quincunx by use of linear optical elements. *J. Opt. Soc. Am. B* **22**, 499–504 (2005).
14. H. B. Perets, Y. Lahini, F. Pozzi, M. Sorel, R. Morandotti, Y. Silberberg, Realization of quantum walks with negligible decoherence in waveguide lattices. *Phys. Rev. Lett.* **100**, 170506 (2008).
15. P. L. Knight, E. Roldán, J. E. Sipe, Quantum walk on the line as an interference phenomenon. *Phys. Rev. A* **68**, 020301 (2003).
16. M. Walschaers, F. Schlawin, T. Wellens, A. Buchleitner, Quantum transport on disordered and noisy networks: An interplay of structural complexity and uncertainty. *Annu. Rev. Condens. Matter Phys.* **7**, 223–248 (2016).
17. K. Mayer, M. C. Tichy, F. Mintert, T. Konrad, A. Buchleitner, Counting statistics of many-particle quantum walks. *Phys. Rev. A* **83**, 062307 (2011).
18. A. M. Childs, D. Gosset, Z. Webb, Universal computation by multiparticle quantum walk. *Science* **339**, 791–794 (2013).
19. J. K. Gamble, M. Friesen, D. Zhou, R. Joynt, S. N. Coppersmith, Two-particle quantum walks applied to the graph isomorphism problem. *Phys. Rev. A* **81**, 052313 (2010).
20. A. Peruzzo, M. Lobino, J. C. F. Matthews, N. Matsuda, A. Politi, K. Poulios, X.-Q. Zhou, Y. Lahini, N. Ismail, K. Wörhoff, Y. Bromberg, Y. Silberberg, M. G. Thompson, J. L. O'Brien, Quantum walks of correlated photons. *Science* **329**, 1500–1503 (2010).
21. J. M. Harrison, J. P. Keating, J. M. Robbins, Quantum statistics on graphs. *Proc. R. Soc. A* **467**, 212–233 (2010).
22. M. B. Plenio, S. F. Huelga, Dephasing-assisted transport: Quantum networks and biomolecules. *New J. Phys.* **10**, 113019 (2008).
23. M. Mohseni, P. Rebentrost, S. Lloyd, A. Aspuru-Guzik, Environment-assisted quantum walks in photosynthetic energy transfer. *J. Chem. Phys.* **129**, 174106 (2008).
24. D. N. Biggerstaff, R. Heilmann, A. A. Zecevik, M. Gräfe, M. A. Broome, A. Fedrizzi, S. Nolte, A. Szameit, A. G. White, I. Kassal, Enhancing coherent transport in a photonic network using controllable decoherence. *Nat. Commun.* **7**, 11282 (2016).
25. J. M. Harrison, J. P. Keating, J. M. Robbins, A. Sawicki, n-particle quantum statistics on graphs. *Commun. Math. Phys.* **330**, 1293–1326 (2014).
26. A. M. Childs, R. Cleve, E. Deotto, E. Farhi, S. Gutmann, D. A. Spielman, in *Conference Proceedings of the Annual ACM Symposium on Theory of Computing* (Association for Computing Machinery, 2003), pp. 59–68.
27. K. Poulios, R. Keil, D. Fry, J. D. A. Meinecke, J. C. F. Matthews, A. Politi, M. Lobino, M. Gräfe, M. Heinrich, S. Nolte, A. Szameit, J. L. O'Brien, Quantum walks of correlated photon pairs in two-dimensional waveguide arrays. *Phys. Rev. Lett.* **112**, 143604 (2014).
28. O. Boada, A. Celi, J. I. Latorre, M. Lewenstein, Quantum simulation of an extra dimension. *Phys. Rev. Lett.* **108**, 133001 (2012).
29. L. Yuan, Q. Lin, M. Xiao, S. Fan, Synthetic dimension in photonics. *Optica* **5**, 1396–1405 (2018).
30. E. Lustig, S. Weimann, Y. Plotnik, Y. Lumer, M. A. Bandres, A. Szameit, M. Segev, Photonic topological insulator in synthetic dimensions. *Nature* **567**, 356–360 (2019).
31. O. Zilberberg, S. Huang, J. Guglielmon, M. Wang, K. P. Chen, Y. E. Kraus, M. C. Rechtsman, Photonic topological boundary pumping as a probe of 4D quantum Hall physics. *Nature* **553**, 59–62 (2018).
32. A. Szameit, S. Nolte, Discrete optics in femtosecond-laser-written photonic structures. *J. Phys. B Atom. Mol. Opt. Phys.* **43**, 163001 (2010).
33. R. Ulrich, M. Johnson, Single-mode fiber-optical polarization rotator. *Appl. Optics* **18**, 1857–1861 (1979).
34. C. Dittel, R. Keil, G. Weihs, Many-body quantum interference on hypercubes. *Quantum Sci. Technol.* **2**, 015003 (2017).
35. C. K. Hong, Z. Y. Ou, L. Mandel, Measurement of subpicosecond time intervals between two photons by interference. *Phys. Rev. Lett.* **59**, 2044–2046 (1987).
36. P. Yang, G. R. Burns, J. Guo, T. S. Luk, G. A. Vawter, Femtosecond laser-pulse-induced birefringence in optically isotropic glass. *J. Appl. Phys.* **95**, 5280–5283 (2004).
37. C.-Y. Wang, J. Gao, X.-M. Jin, On-chip rotated polarization directional coupler fabricated by femtosecond laser direct writing. *Opt. Lett.* **44**, 102–105 (2019).
38. G. D. Marshall, A. Politi, J. C. F. Matthews, P. Dekker, M. Ams, M. J. Withford, J. L. O'Brien, Laser written waveguide photonic quantum circuits. *Opt. Express* **17**, 12546–12554 (2009).
39. N. Viggianiello, F. Flamini, L. Innocenti, D. Cozzolino, M. Bentivegna, N. Spagnolo, A. Crespi, D. J. Brod, E. F. Galvão, R. Osellame, F. Sciarrino, Experimental generalized quantum suppression law in Sylvester interferometers. *New J. Phys.* **20**, 033017 (2018).
40. C. Dittel, G. Dufour, M. Walschaers, G. Weihs, A. Buchleitner, R. Keil, Totally destructive many-particle interference. *Phys. Rev. Lett.* **120**, 240404 (2018).
41. C. Dittel, G. Dufour, M. Walschaers, G. Weihs, A. Buchleitner, R. Keil, Totally destructive interference for permutation-symmetric many-particle states. *Phys. Rev. A* **97**, 062116 (2018).
42. J. M. Zeuner, M. C. Rechtsman, R. Keil, F. Dreisow, A. Tünnermann, S. Nolte, A. Szameit, Negative coupling between defects in waveguide arrays. *Opt. Lett.* **37**, 533–535 (2012).
43. R. Keil, C. Poli, M. Heinrich, J. Arkinstant, G. Weihs, H. Schomerus, A. Szameit, Universal sign control of coupling in tight-binding lattices. *Phys. Rev. Lett.* **116**, 213901 (2016).
44. J. M. Leinaas, J. Myrheim, On the theory of identical particles. *Il Nuovo Cim. B* **37**, 1–23 (1977).
45. H. Tang, X.-F. Lin, Z. Feng, J.-Y. Chen, J. Gao, K. Sun, C.-Y. Wang, P.-C. Lai, X.-Y. Xu, Y. Wang, L.-F. Qiao, A.-L. Yang, X.-M. Jin, Experimental two-dimensional quantum walk on a photonic chip. *Sci. Adv.* **4**, eaat3174 (2018).
46. Z.-Q. Jiao, J. Gao, W.-H. Zhou, X.-W. Wang, R.-J. Ren, X.-Y. Xu, L.-F. Qiao, X.-M. Jin, Two-dimensional quantum walk of correlated photons. arXiv:2007.06554 (2020).
47. L. Sansoni, F. Sciarrino, G. Vallone, P. Mataloni, A. Crespi, R. Ramponi, R. Osellame, Two-particle bosonic-fermionic quantum walk via integrated photonics. *Phys. Rev. Lett.* **108**, 010502 (2012).
48. J. C. F. Matthews, K. Poulios, J. D. A. Meinecke, A. Politi, A. Peruzzo, N. Ismail, K. Wörhoff, M. G. Thompson, J. L. O'Brien, Observing fermionic statistics with photons in arbitrary processes. *Sci. Rep.* **3**, 1539 (2013).
49. O. Boada, A. Celi, J. Rodríguez-Laguana, J. I. Latorre, M. Lewenstein, Quantum simulation of non-trivial topology. *New J. Phys.* **17**, 045007 (2015).
50. R. Heilmann, M. Gräfe, S. Nolte, A. Szameit, Arbitrary photonic wave plate operations on chip: Realizing Hadamard, Pauli-X, and rotation gates for polarisation qubits. *Sci. Rep.* **4**, 4118 (2014).
51. L. A. Fernandes, J. R. Grenier, P. R. Herman, J. S. Aitchison, P. V. S. Marques, Femtosecond laser fabrication of birefringent directional couplers as polarization beam splitters in fused silica. *Opt. Express* **19**, 11992–11999 (2011).
52. Y. Bromberg, Y. Lahini, R. Morandotti, Y. Silberberg, Quantum and classical correlations in waveguide lattices. *Phys. Rev. Lett.* **102**, 253904 (2009).
53. M. C. Tichy, M. Tiersch, F. Mintert, A. Buchleitner, Many-particle interference beyond many-boson and many-fermion statistics. *New J. Phys.* **14**, 093015 (2012).
54. J. L. Walsh, A closed set of normal orthogonal functions. *Am. J. Math.* **45**, 5–24 (1923).

Acknowledgments: We thank C. Otto for preparing the high-quality fused silica samples used for the inscription of all photonic structures used in this work. **Funding:** We acknowledge funding from the European Union Horizon 2020 program (ErBeStA 800942), the Deutsche Forschungsgemeinschaft (grants SZ 276/12-1, BL 574/13-1, SZ 276/15-1, SZ 276/20-1, and SZ 276/21-1), the Austrian Science Fund (grant P 30459), the Georg H. Endress Foundation, and the Alfred Krupp von Bohlen und Halbach Foundation. **Author contributions:** R.K. developed the theoretical framework of polarization coupling in waveguide circuits. M.E. performed the experiments and refined the theoretical model. M.E., M.H. L.J.M., and A.S. interpreted the measurement data. A.S. supervised the project. C.D. provided analysis tools and discussed the data. All authors discussed the results and cowrote the paper. **Competing interests:** The authors declare that they have no competing interests. **Data and materials availability:** All data needed to evaluate the conclusions in the paper are present in the paper and/or the Supplementary Materials. Additional data related to this paper may be requested from the authors.

Submitted 29 April 2020
 Accepted 13 January 2021
 Published 26 February 2021
 10.1126/sciadv.abc5266

Citation: M. Ehrhardt, R. Keil, L. J. Maczewsky, C. Dittel, M. Heinrich, A. Szameit, Exploring complex graphs using three-dimensional quantum walks of correlated photons. *Sci. Adv.* **7**, eabc5266 (2021).